

Sliding-induced ferrovalley polarization and possible antiferromagnetic half-metal in bilayer altermagnets

Xin Zhang¹ (张鑫) and Shihao Zhang^{2,†} (张世豪)

- 1 School of Physical Science and Technology, Kunming University, Kunming 650214, China
- 2 School of Physics and Electronics, Hunan University, Changsha 410082, China
Corresponding author. E-mail: †zhangshh@hnu.edu.cn

ABSTRACT

Altermagnets, a newly discovered class of materials, exhibit zero net magnetization while hosting spin-split electronic bands. However, monolayer altermagnets maintain degenerate band gaps at the high-symmetry X and Y points in the Brillouin zone, manifesting a paravalley phase characterized by unpolarized valley states. In this work, we demonstrate that spontaneously broken valley degeneracy can be achieved through interlayer sliding in engineered M_2A_2B and $M_2AA'B$ bilayer altermagnets by first-principles calculations and minimal microscopic model. We propose a promising route to achieve antiferromagnetic half-metal driven by sliding and emergent ferrovalley phase without applied electric field, which is realized in the V_2SSeO engineered bilayer. Our calculations also reveal that Mo_2O_2O exhibits the largest valley splitting gap of ~ 0.31 eV, making it a promising candidate for valley-spin valve devices. Furthermore, band structure calculations on $Mo_2AA'O$ materials demonstrate that increasing the difference in atomic number (ΔZ) between A and A' site atoms effectively enhances valley polarization. This work establishes a novel platform for discovering and controlling ferrovalley states in altermagnetic systems.

Keywords altermagnets, interlayer sliding, ferrovalley polarization

1 Introduction

Altermagnets (AMs) represent a newly discovered third fundamental magnetic phase beyond ferromagnets and antiferromagnets. It maintains vanishing net magnetization (characteristic of antiferromagnets) while exhibiting momentum-dependent spin-splitting electronic bands (a hallmark of ferromagnets) [1-12]. Consequently, the emergence of altermagnetism has thus sparked extensive investigations, with hallmark phenomena receiving robust confirmation through theoretical calculations and experimental probes: symmetry-breaking lifted Kramers degeneracy [13, 14], Berry-curvature-driven anomalous Hall/Nernst/thermal Hall effects [15-24], crystal-symmetry-enabled nonrelativistic spin currents [25], magneto-optical responses [26, 27], and topologically protected chiral magnon excitations [28, 29]. Simultaneously, altermagnets enable access to enriched physical phenomena, such as valley polarization and multipiezo effects, through diverse external control methods including strain engineering [30-32], electric-field gating [31, 33-36], magnetic-field tuning [18, 30, 37-39], and optical excitation [40]. However, such externally controlled phenomena are inherently volatile, as their effects cease abruptly upon the removal of the applied fields. This necessitates the pursuit of intrinsically nonvolatile material platforms. Inspired by sliding-engineered

ferrovalley polarization in Fe_2MX_4 systems [41], we constructed interlayer-sliding bilayers from monolayer altermagnetic semiconductors $\text{M}_2\text{A}_2\text{B}$ and $\text{M}_2\text{AA}'\text{B}$ ($\text{M} = \text{Ti, V, Cr, Mn, Fe, Mo}$; $\text{A, A}' = \text{O, S, Se, Te}$) [42]. Through first-principles calculations, we identified compounds exhibiting spontaneous ferrovalley polarization.

In the momentum space of many two-dimensional materials, such as graphene and transition metal dichalcogenides (TMDs), the energy extrema often appear in pairs located at specific high-symmetry points of the Brillouin zone, most commonly denoted as the K and K' valleys [43-45]. The electron populations in the two valleys remain equal due to time-reversal symmetry, resulting in a nonpolarized paravalley state. Valley polarization occurs when an external or internal mechanism breaks this symmetry, causing carriers to preferentially occupy one valley, thereby lifting the valley degeneracy [43, 46-48]. This polarized valley degree of freedom can serve as a novel information carrier, analogous to electronic charge or spin. For example, defining the K valley as logic “1” and K' valley as “0” offers a route to encode information, enabling the development of valleytronic devices for data processing, storage, and transmission. Ferrovalley materials represent a distinct class of systems that intrinsically break valley degeneracy by stabilizing one valley at a lower energy than the other, resulting in spontaneous valley polarization without external magnetic field [41, 49]. By combining ferromagnetic order and the valley degree of freedom, such materials provide a promising platform for designing next generation electronic devices with low energy consumption.

In this work, we designed x -sliding bilayer altermagnets based on $\text{M}_2\text{A}_2\text{B}$ and $\text{M}_2\text{AA}'\text{B}$ prototypes by first-principles calculations. We propose a minimal microscopic model to describe the ferrovalley states in the bilayer altermagnets. In the family of sliding bilayer altermagnets, V_2SSeO bilayer may achieve antiferromagnetic half-metal induced by sliding operation and emergent ferrovalley mechanism without applied electric field. Furthermore, we performed high-throughput computational screening, and found a series of compounds exhibiting spontaneous valley polarization. And our calculations show that increasing the difference in atomic number (ΔZ) between A and A' site atoms effectively enhances valley polarization. More detailed discussions are presented in the following.

2 Computational methods

Our computational framework leveraged the DS-PAW module within the Device Studio platform, implementing density functional theory (DFT) with projector-augmented wave method for sliding configurations [50, 51]. The electron exchange and correlations were described by Perdew-Burke-Ernzerhof (PBE) function. In all calculations, the convergence criteria were set to 10^{-6} eV for total energy and 0.05 eV/Å for atomic forces, with a plane-wave energy cutoff of 600 eV. Moreover, a vacuum region of about 20 Å was included to eliminate spurious interactions between periodic layers. The van der Waals interaction between the two layers was accounted for using the DFT-D3 method with Becke-Johnson damping [52]. The Brillouin zone was sampled using a Γ -centered $7 \times 7 \times 1$ Monkhorst-Pack k-point grid [53]. DFT+U calculations were performed with an effective Hubbard parameter $U_{\text{eff}} = U - J = 3$ eV on the d-orbitals of M atoms [54, 55] to include on-site Hubbard interaction.

3 Results and discussion

M_2A_2B and $M_2AA'B$ have identical crystal structures, with the A' atom in $M_2AA'B$ being chemically equivalent to the A atom. The monolayer $M_2AA'B$ systems exhibit the structure shown in Fig. 1(a), the M - B atomic plane is sandwiched between A and A' atomic planes, similar to the monolayer V_2STeO [30] and V_2SeTeO [56, 57]. The spins of M atoms are denoted by orange arrows, exhibiting A-type antiferromagnetic ordering. Remarkably, specific elemental combinations enable single-layer materials to function as altermagnets [42]. Fig. 1(b) displays AA-stacked bilayer configuration without sliding, which exhibits paravalley characteristic via preserved σ_D crystalline mirror symmetry [41]. In order to break σ_D symmetry and achieve ferrovalley states, we engineered bilayer systems with orthogonal sliding configurations: x -sliding ($\delta x = a/2$) and y -sliding ($\delta y = b/2$), where one layer undergoes half-lattice-constant displacement relative to the other along corresponding crystal axes, as illustrated in Fig. 1(c) and 1(d).

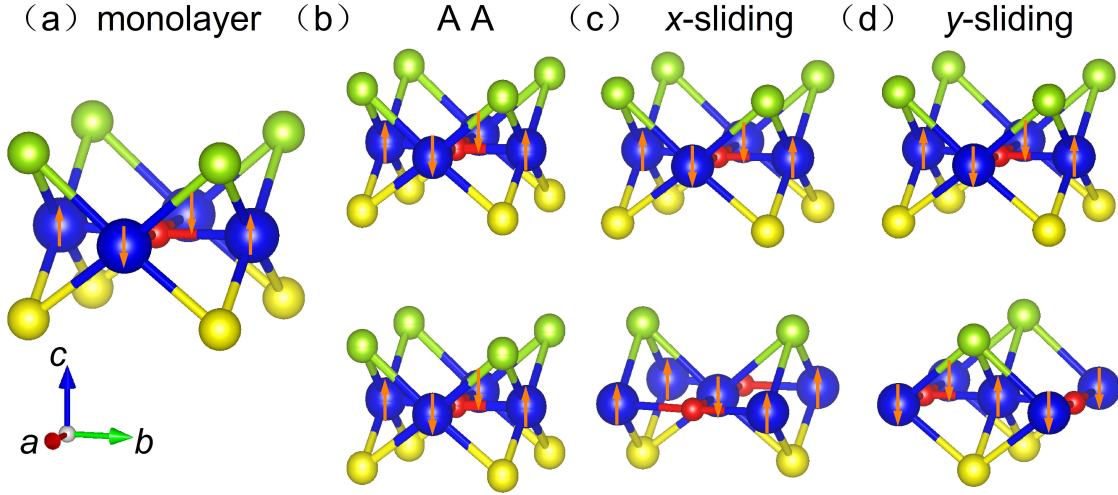


Fig. 1 Schematic structures of M_2A_2B and $M_2AA'B$. Blue spheres represent M atoms, green and yellow spheres represent A and A' atoms, and red spheres represent B atoms. (a) Monolayer structure. Antiferromagnetic spins on M atoms are indicated by orange arrows on blue spheres. (b) AA-stacked bilayer structure without interlayer sliding. (c) Bilayer stacking structure with half-lattice-constant sliding along the x -axis direction. (d) Bilayer stacking structure with half-lattice-constant sliding along the y -axis direction.

We begin discussions about ferrovalley physics with V_2SSeO system. Fig. 2 shows the calculated electronic band structure of V_2SSeO . As shown in Fig. 2(a), monolayer structure holds direct bandgaps of 214 meV at the X and Y points. Altermagnetism is demonstrated by spin splitting $\sim (k_x^2 - k_y^2)$ in the energy bands, while identical band gaps without spin polarization indicate of paravalley state. Because of $C_{4z}\mathcal{T}$ symmetry, the conduction band minimums at the X and Y points are mainly contributed by d_{xz} and d_{yz} orbitals of different sublattices, respectively. The valence band maximums originate from hybridization of d_{xy} and p orbitals. In the AA-stacking bilayer, the bandgaps are drastically reduced by interlayer interaction as shown in Fig. 2(b).

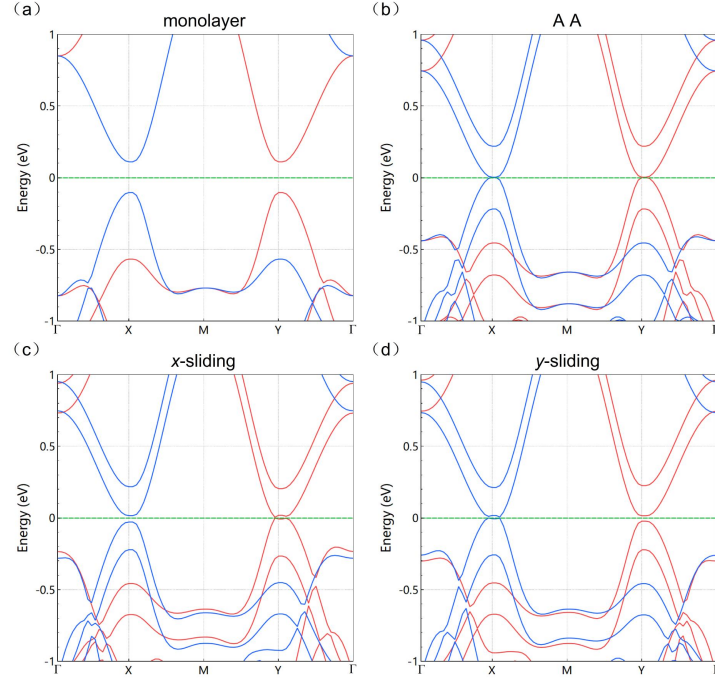


Fig. 2 Electronic band structures of V₂SSeO: (a) monolayer, (b) AA bilayer, (c) *x*-sliding bilayer and (d) *y*-sliding bilayer. The spin-up and spin-down channels are represented by red and blue curves, respectively.

Spin polarization arises in the *x*-sliding bilayer, with the spin-down band at X valley opening a larger gap than the spin-up band at Y valley, yielding a Δ_{gap} ($\Delta_{\text{gap}} = \Delta E_X - \Delta E_Y \approx 18.5$ meV, see in Fig. 2(c)). The ferrovalley state is antiferromagnetic half-metal, conducting only in one spin channel. Crucially, the observed band inversion in the Y valley provides evidence of nontrivial topological state. Meanwhile, the *y*-sliding bilayer exhibits reversed valley polarization as shown in Fig. 2(d). The two sliding configurations yield antiferromagnetic half-metal with valley polarization with Δ_{gap} values of opposite signs.

Now we use one minimal model to describe the electronic structures of aforementioned different configurations. We begin with monolayer's effective Hamiltonian [58],

$$H_0 = [\mu + A(\cos k_x + \cos k_y)]\tau_0\sigma_0 + (\cos k_x - \cos k_y)(B\tau_z\sigma_0 + C\tau_0\sigma_z) \\ + t\cos\frac{k_x}{2}\cos\frac{k_y}{2}\tau_x\sigma_0 + [u + D(\cos k_x + \cos k_y)]\tau_z\sigma_z.$$

Here τ and σ denote the Pauli matrices in the sublattice and spin space, respectively. It holds the mirror crystalline symmetry and $C_{4z}\mathcal{T}$ symmetry. In this work, we ignore the spin-orbit coupling for simplicity. $(\cos k_x - \cos k_y)$ term refers to the spin-degenerate bands along $\Gamma - M$ direction. This microscopic model gives out the alternating energy bands as shown in Fig. 3(a). In the AA-stacking configuration, the effective Hamiltonian can be written as $H = H_0l_0 + t'\tau_0\sigma_0l_x$, where l is the Pauli matrix defined in the layer space and t' is the interlayer hopping. As shown in the Fig. 3(b), the bilayer's electronic structure evolves into layer-splitting energy bands with smaller bandgap. But in the *x*-sliding or *y*-sliding bilayer structure, mirror symmetry is broken and the spin-degenerate bands along $\Gamma - M$ direction are also split. In the *x*-sliding bilayer configuration, the effective Hamiltonian becomes $H = H_0l_0 + t'\tau_0\sigma_0l_x + t''\tau_z\sigma_0l_0 + t_p\cos k_x\tau_z\sigma_zl_0$. In the *y*-sliding bilayer configuration, the effective Hamiltonian is rewritten as $H = H_0l_0 + t'\tau_0\sigma_0l_x - t''\tau_z\sigma_0l_0 +$

$t_p \cos k_y \tau_z \sigma_z l_0$. As shown in the Fig. 3(c, d), the bilayer's energy bands are driven into ferrovalley states by sliding operation.

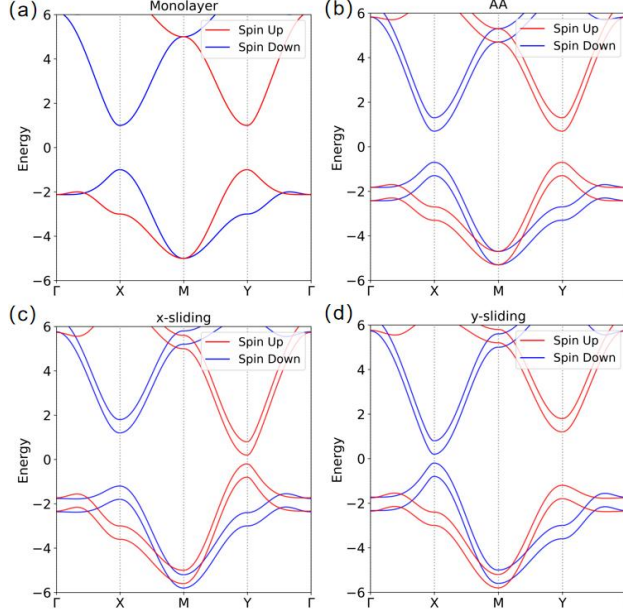


Fig. 3 Band structures of different configurations. We use the set of parameters: $A = C = -B/2 = D/2 = \mu/2 = t/8 = -u/6 = 0.5$, and $t' = -0.3, t'' = -0.1, t_p = 0.4$.

Given the identical properties of x -sliding and y -sliding bilayers, we exclusively computed the band structure for the constructed x -sliding bilayer in our material simulations. We performed high-throughput calculations to discover more potential altermagnets with remarkable ferrovalley feature. Inspired by recent theoretical work about altermagnet monolayers [42], we focus on the M_2A_2B and Janus $M_2AA'B$ altermagnets because of their possible direct-gap electronic structures. The calculated electronic valley polarizations are summarized in Table 1. As shown in Table 1, many bilayers exhibit metallic electronic structures, because the interlayer coupling reduces the bandgaps. Only few bilayers still keep semiconducting behavior. These semiconducting variants display polarized ferrovalley characteristics, exhibiting Δ_{gap} values ranging from several to tens of meV. $\text{Mo}_2\text{O}_2\text{O}$ constitutes the sole exception to this trend, possessing a substantially larger Δ_{gap} of 312.3 meV (Fig. 4), which notably exceeds the reported value of 290 meV for bilayer Fe_2WTe_4 [41], thereby establishing an ideal platform for investigating valley spin valves. The screened AM materials consistently exhibit lower energy than their ferromagnetic (FM) counterparts (Table S1), demonstrating the stability of the AM state.

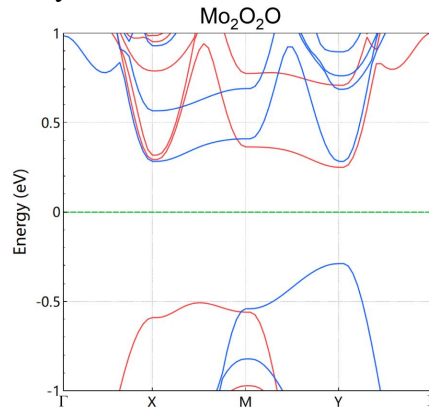


Fig. 4 The electronic band structures of bilayer $\text{Mo}_2\text{O}_2\text{O}$. The spin-up and spin-down bands are represented by red and blue lines, respectively.

Table 1 The Δ_{gap} values (eV) calculated for the constructed bilayer altermagnet materials. Here “/” refers to metallic electronic structure of bilayer altermagnet.

Materials	Δ_{gap} (eV)	Materials	Δ_{gap} (eV)	Materials	Δ_{gap} (eV)
Ti ₂ O ₂ O	/	V ₂ OSSe	/	V ₂ SSeO	0.0458
V ₂ O ₂ O	/	Ti ₂ OSeO	/	Cr ₂ SSeO	/
Cr ₂ O ₂ O	/	V ₂ OSeO	0.0018	Mo ₂ SSeO	0.0093
Mo ₂ O ₂ O	0.3123	Cr ₂ OSeO	/	Ti ₂ SSeSe	/
V ₂ S ₂ O	0.0170	Mo ₂ OSeO	/	V ₂ SSeSe	/
Cr ₂ S ₂ O	/	Fe ₂ OSeS	/	V ₂ SSeTe	/
Mo ₂ S ₂ O	/	Cr ₂ OSeSe	/	Cr ₂ STeO	/
V ₂ Se ₂ O	0.0454	Fe ₂ OSeSe	/	Mo ₂ STeO	0.0129
Cr ₂ Se ₂ O	/	Mn ₂ OSeTe	/	Ti ₂ STeS	/
Mo ₂ Se ₂ O	0.0041	Ti ₂ OTeO	/	V ₂ STeS	/
Cr ₂ Te ₂ O	/	V ₂ OTeO	/	Ti ₂ STeSe	/
Mo ₂ Te ₂ O	/	Cr ₂ OTeO	/	V ₂ STeSe	/
Ti ₂ OSO	/	Mo ₂ OTeO	/	V ₂ STeTe	/
V ₂ OSO	0.0017	Fe ₂ OTeS	/	Cr ₂ SeTeO	/
Cr ₂ OSO	/	Fe ₂ OTeSe	/	Mo ₂ SeTeO	0.0064
Mo ₂ OSO	0.0022	Ti ₂ OTeTe	/	Ti ₂ SeTeSe	/
Cr ₂ OSS	/	Mn ₂ OTeTe	/	V ₂ SeTeTe	/

Fig. 5 presents the electronic band structures of Mo₂Se₂O, Mo₂SeTeO, and Mo₂STeO. All compounds exhibit spin-split bands characteristic of altermagnetism. Crucially, the contrasting bandgap magnitudes between spin-up (spin-down) at X point and spin-down (spin-up) at Y point demonstrate polarized ferrovalley properties. As seen in Table 1, the bandgap follows a clear ascending order from Mo₂Se₂O to Mo₂SeTeO to Mo₂STeO, tracking the increasing atomic number difference (ΔZ) between chalcogen sites A and A', which provides a new avenue for discovering materials with enhanced valley polarization.

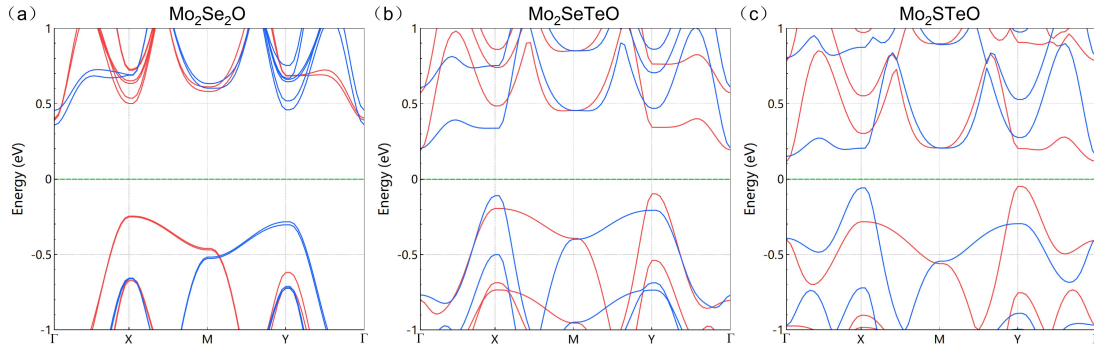


Fig. 5 The electronic band structures of bilayer (a) Mo₂Se₂O, (b) Mo₂SeTeO and (c) Mo₂STeO. Spin-up and spin-down channels are represented by red and blue curves, respectively.

We noted that the choice of vdw functionals and Hubbard parameters always influence the calculated bandgaps. However, in this work, we propose a promising route to achieve antiferromagnetic half-metal driven by sliding and emergent ferrovalley phase without applied electric field. By tuning the direction of sliding operation, we can achieve the spin valve with conducting spin-up or spin-down electrons. More importantly, the spin valve has zero net spin moment and then no impact on nearby spintronic components, which promises the robust application in the integrated spintronic devices.

4 Conclusions

In conclusion, we designed x -sliding bilayer altermagnets based on M_2A_2B and $M_2AA'B$ prototypes. We propose a minimal microscopic model to describe the ferrovalley states in the bilayer altermagnets. In the family of sliding bilayer altermagnets, our calculations reveal that V_2SSeO bilayer may achieve antiferromagnetic half-metal induced by sliding operation and emergent ferrovalley mechanism. Computational screening identified a series of compounds exhibiting spontaneous valley polarization, with Mo_2O_2O showing the largest valley polarization of ~ 0.31 eV. This system offers a promising platform for spin valve applications and provides valuable guidance for further exploration of altermagnetic materials.

Declarations The authors declare that they have no competing interests and there are no conflicts.

Acknowledgements This work was supported by the National Natural Science Foundation of China (Grant No. 12304217), the Special Basic Cooperative Research Programs of Yunnan Provincial Undergraduate Universities' Association (Grant No. 202401BA070001-013), the Scientific Research Fund of Yunnan Provincial Department of Education (Grant No. 2024J0778), the National Key Research and Development Program of China (Grant No. 2024YFA1410300), the Natural Science Foundation of Hunan Province (Grant No. 2025JJ60002), and the Fundamental Research Funds for the Central Universities from China (Grant No. 531119200247). We gratefully acknowledge HZWTECH for providing computation facilities.

References

1. L. Šmejkal, J. Sinova and T. Jungwirth, Beyond Conventional Ferromagnetism and Antiferromagnetism: A Phase with Nonrelativistic Spin and Crystal Rotation Symmetry, *Physical Review X* 12, 031042 (2022).
2. L. Šmejkal, J. Sinova and T. Jungwirth, Emerging Research Landscape of Altermagnetism, *Physical Review X* 12, 040501 (2022).
3. X. Chen, J. Ren, Y. Zhu, Y. Yu, A. Zhang, P. Liu, J. Li, Y. Liu, C. Li, and Q. Liu, Enumeration and representation theory of spin space groups, *Phys. Rev. X* 14, 031038 (2024).
4. X. Chen, Y. Liu, P. Liu, Y. Yu, J. Ren, J. Li, A. Zhang, and Q. Liu, Unconventional magnons in collinear magnets dictated by spin space groups, *Nature* 640, 349 (2025).
5. X. Duan, J. Zhang, Z. Zhu, Y. Liu, Z. Zhang, I. Žutić, and Tong Zhou, Antiferroelectric altermagnets: antiferroelectricity alters magnets, *Phys. Rev. Lett.* 134, 106801 (2025).
6. M. Gu, Y. Liu, H. Zhu, K. Yananose, X. Chen, Y. Hu, A. Stroppa, and Q. Liu, Ferroelectric switchable altermagnetism, *Phys. Rev. Lett.* 134, 106802 (2025).
7. S. Qu, X.-Y. Hou, Z.-X. Liu, P.-J. Guo and Z.-Y. Lu, Altermagnetic Weyl node-network metals protected by spin symmetry, *Physical Review B* 111, 195138 (2025).
8. Y. Che, H. Lv, X. Wu and J. Yang, Engineering Altermagnetic States in Two-Dimensional Square Tessellations, *Physical Review Letters* 135, 036701 (2025).

9. J. Zhou and C. Zhang, Contrasting Light-Induced Spin Torque in Antiferromagnetic and Altermagnetic Systems, *Physical Review Letters* 134, 176902 (2025).
10. H.-Y. Ma, M. Hu, N. Li, J. Liu, W. Yao, J.-F. Jia and J. Liu, Multifunctional antiferromagnetic materials with giant piezomagnetism and noncollinear spin current, *Nature Communications* 12, 2846 (2021).
11. B. Jiang, M. Hu, J. Bai, Z. Song, C. Mu, G. Qu, W. Li, W. Zhu, H. Pi, Z. Wei, Y.-J. Sun, Y. Huang, X. Zheng, Y. Peng, L. He, S. Li, J. Luo, Z. Li, G. Chen, H. Li, H. Weng and T. Qian, A metallic room-temperature d-wave altermagnet, *Nature Physics* 21, 754 (2025).
12. X. He and S. Zhang, Dirac fermions in the altermagnet Ce_4Sb_3 , *Physical Review B* 112, 075138 (2025).
13. T. Osumi, S. Souma, T. Aoyama, K. Yamauchi, A. Honma, K. Nakayama, T. Takahashi, K. Ohgushi and T. Sato, Observation of a giant band splitting in altermagnetic MnTe, *Physical Review B* 109, 115102 (2024).
14. J. Ding, Z. Jiang, X. Chen, Z. Tao, Z. Liu, T. Li, J. Liu, J. Sun, J. Cheng, J. Liu, Y. Yang, R. Zhang, L. Deng, W. Jing, Y. Huang, Y. Shi, M. Ye, S. Qiao, Y. Wang, Y. Guo, D. Feng and D. Shen, Large Band Splitting in g-Wave Altermagnet CrSb, *Physical Review Letters* 133, 206401 (2024).
15. H. Reichlova, R. Lopes Seeger, R. González-Hernández, I. Kounta, R. Schlitz, D. Kriegner, P. Ritzinger, M. Lammel, M. Leiviskä, A. Birk Hellenes, K. Olejník, V. Petříček, P. Doležal, L. Horak, E. Schmoranzero, A. Badura, S. Bertaina, A. Thomas, V. Baltz, L. Michez, J. Sinova, S. T. B. Goennenwein, T. Jungwirth and L. Šmejkal, Observation of a spontaneous anomalous Hall response in the Mn_5Si_3 d-wave altermagnet candidate, *Nature Communications* 15, 4961 (2024).
16. Z. Feng, X. Zhou, L. Šmejkal, L. Wu, Z. Zhu, H. Guo, R. González-Hernández, X. Wang, H. Yan, P. Qin, X. Zhang, H. Wu, H. Chen, Z. Meng, L. Liu, Z. Xia, J. Sinova, T. Jungwirth and Z. Liu, An anomalous Hall effect in altermagnetic ruthenium dioxide, *Nature Electronics* 5, 735 (2022).
17. T. Tschirner, P. Keßler, R. D. Gonzalez Betancourt, T. Kotte, D. Kriegner, B. Büchner, J. Dufouleur, M. Kamp, V. Jovic, L. Smejkal, J. Sinova, R. Claessen, T. Jungwirth, S. Moser, H. Reichlova and L. Veyrat, Saturation of the anomalous Hall effect at high magnetic fields in altermagnetic RuO_2 , *APL Materials* 11 (2023).
18. X. Hu, W. Zhao, W. Xia, H. Sun, C. Wu, Y.-Z. Wu and P. Li, Valley polarization and anomalous valley Hall effect in altermagnet $\text{Ti}_2\text{Se}_2\text{S}$ with multipiezo properties, *Applied Physics Letters* 127 (2025).
19. M. Leiviskä, J. Rial, A. Bad'ura, R. L. Seeger, I. Kounta, S. Beckert, D. Kriegner, I. Joumard, E. Schmoranzero, J. Sinova, O. Gomonay, A. Thomas, S. T. B. Goennenwein, H. Reichlová, L. Šmejkal, L. Michez, T. Jungwirth and V. Baltz, Anisotropy of the anomalous Hall effect in thin films of the altermagnet candidate Mn_5Si_3 , *Physical Review B* 109, 224430 (2024).
20. Y. Bai, X. Xiang, S. Pan, S. Zhang, H. Chen, X. Chen, Z. Han, G. Xu and F. Xu, Nonlinear field dependence of Hall effect and high-mobility multi-carrier transport in an altermagnet CrSb, *Applied Physics Letters* 126 (2025).
21. X. Zhou, W. Feng, R.-W. Zhang, L. Šmejkal, J. Sinova, Y. Mokrousov and Y. Yao, Crystal Thermal Transport in Altermagnetic RuO_2 , *Physical Review Letters* 132, 056701 (2024).
22. X.-J. Yi, Y. Mao, X. Lu and Q.-F. Sun, Spin splitting Nernst effect in altermagnets, *Physical Review B* 111, 035423 (2025).
23. L. Han, X. Z. Fu, W. Q. He, J. K. Dai, Y. X. Zhu, W. F. Yang, Y. L. Chen, J. C. Zhang, W. X. Zhu, H. Bai, C. Chen, D. Z. Hou, C. H. Wan, X. F. Han, C. Song, J.

- W. Liu and F. Pan, Nonvolatile anomalous Nernst effect in Mn_5Si_3 with a collinear Neel vector, *Physical Review Applied* 23, 044066 (2025).
24. Chao-Yang Tan, Panjun Feng, Ze-Feng Gao, Fengjie Ma, Peng-Jie Guo and Z.-Y. Lu, Stacking-induced type-II quantum spin Hall insulators with high spin Chern number in unconventional magnetism, arXiv:2508.05365 (2025).
 25. Chang Pan, Shuai Hu, Fanli Yang, W. F. Dongchao Yang, Zhong Shi, Liqing Pan and X. Q. Shiming Zhou, Unveiling the nonrelativistic spin current polarization in an altermagnet, arXiv:2412.18937v1 (2024).
 26. I. Gray, Q. Deng, Q. Tian, M. Chilcote, J. S. Dodge, M. Brahlek and L. Wu, Time-resolved magneto-optical effects in the altermagnet candidate MnTe, *Applied Physics Letters* 125 (2024).
 27. M. Vila, V. Sunko and J. E. Moore, Orbital-spin locking and its optical signatures in altermagnets, *Physical Review B* 112, L020401 (2025).
 28. L. Šmejkal, A. Marmodoro, K.-H. Ahn, R. González-Hernández, I. Turek, S. Mankovsky, H. Ebert, S. W. D'Souza, O. Šipr, J. Sinova and T. Jungwirth, Chiral Magnons in Altermagnetic RuO_2 , *Physical Review Letters* 131, 256703 (2023).
 29. Z. Liu, M. Ozeki, S. Asai, S. Itoh and T. Masuda, Chiral Split Magnon in Altermagnetic MnTe, *Physical Review Letters* 133, 156702 (2024).
 30. Y. Chang, Y. Wu, L. Deng, X. Yin and X. Zhang, Valley-Related Multipiezo Effect in Altermagnet Monolayer V_2SeTeO , *Materials* 18, 527 (2025).
 31. I. Khan, D. Bezzerga, B. Marfoua and J. Hong, Altermagnetism, piezovallay, and ferroelectricity in two-dimensional Cr_2SeO altermagnet, *npj 2D Materials and Applications* 9, 18 (2025).
 32. B. Marfoua and J. Hong, Strain-dependent Rashba effect, and spin Hall conductivity in the altermagnetic Janus V_2SeTeO monolayer, *Current Applied Physics* 69, 47 (2025).
 33. H. Sun, P. Dong, C. Wu and P. Li, Multifield-induced antiferromagnet transformation into altermagnet and realized anomalous valley Hall effect in monolayer VPSe_3 , *Physical Review B* 111, 235431 (2025).
 34. D. Wang, H. Wang, L. Liu, J. Zhang and H. Zhang, Electric-Field-Induced Switchable Two-Dimensional Altermagnets, *Nano Letters* 25, 498 (2025).
 35. S.-D. Guo, Y. Liu, J. Yu and C.-C. Liu, Valley polarization in twisted altermagnetism, *Physical Review B* 110, L220402 (2024).
 36. S.-D. Guo and Y. S. Ang, Spontaneous spin splitting in electric potential difference antiferromagnetism, *Physical Review B* 108, L180403 (2023).
 37. P. Rao, A. Mook and J. Knolle, Tunable band topology and optical conductivity in altermagnets, *Physical Review B* 110, 024425 (2024).
 38. A. R. Chakraborty, J. Schmalian and R. M. Fernandes, Magnetic-field-tuned randomness in inhomogeneous altermagnets, *Physical Review B* 112, 035146 (2025).
 39. Y. Wu, L. Deng, X. Yin, J. Tong, F. Tian and X. Zhang, Valley-Related Multipiezo Effect and Noncollinear Spin Current in an Altermagnet $\text{Fe}_2\text{Se}_2\text{O}$ Monolayer, *Nano Letters* 24, 10534 (2024).
 40. M. Weber, S. Wust, L. Haag, A. Akashdeep, K. Leckron, C. Schmitt, R. Ramos, T. Kikkawa, E. Saitoh, M. Kläui, L. Šmejkal, J. Sinova, M. Aeschlimann, G. Jakob, B. Stadtmüller and H. C. Schneider, All optical excitation of spin polarization in d-wave altermagnets, arXiv:2408.05187v1 (2024).
 41. Y.-Q. Li, Y.-K. Zhang, X.-L. Lu, Y.-P. Shao, Z.-Q. Bao, J.-D. Zheng, W.-Y. Tong and C.-G. Duan, Ferrovalley Physics in Stacked Bilayer Altermagnetic Systems, *Nano Letters* 25, 6032 (2025).

42. R. Xu, Y. Gao and J. Liu, Chemical design of monolayer altermagnets, *arXiv*: 2505.15484v1 (2025).
43. D. Xiao, W. Yao and Q. Niu, Valley-Contrasting Physics in Graphene: Magnetic Moment and Topological Transport, *Physical Review Letters* 99, 236809 (2007).
44. A. H. Castro Neto, F. Guinea, N. M. R. Peres, K. S. Novoselov and A. K. Geim, The electronic properties of graphene, *Reviews of Modern Physics* 81, 109 (2009).
45. T. Cao, G. Wang, W. Han, H. Ye, C. Zhu, J. Shi, Q. Niu, P. Tan, E. Wang, B. Liu and J. Feng, Valley-selective circular dichroism of monolayer molybdenum disulphide, *Nature Communications* 3, 887 (2012).
46. H. Zeng, J. Dai, W. Yao, D. Xiao and X. Cui, Valley polarization in MoS₂ monolayers by optical pumping, *Nature Nanotechnology* 7, 490 (2012).
47. D. Xiao, G.-B. Liu, W. Feng, X. Xu and W. Yao, Coupled Spin and Valley Physics in Monolayers of MoS₂ and Other Group-VI Dichalcogenides, *Physical Review Letters* 108, 196802 (2012).
48. S. Wu, J. S. Ross, G.-B. Liu, G. Aivazian, A. Jones, Z. Fei, W. Zhu, D. Xiao, W. Yao, D. Cobden and X. Xu, Electrical tuning of valley magnetic moment through symmetry control in bilayer MoS₂, *Nature Physics* 9, 149 (2013).
49. S.-D. Guo, L. Zhang, Y. Zhang, P. Li and G. Wang, Large spontaneous valley polarization and anomalous valley Hall effect in antiferromagnetic monolayer Fe₂CF₂, *Physical Review B* 110, 024416 (2024).
50. P. E. Blöchl, Projector augmented-wave method, *Physical Review B* 50, 17953 (1994).
51. Hongzhiwei Technology, Device Studio, Version V2024A, China, Available online: <<https://cloud.hzwtech.com/web/home>> (2024).
52. S. Grimme, S. Ehrlich and L. Goerigk, Effect of the damping function in dispersion corrected density functional theory, *Journal of Computational Chemistry* 32, 1456 (2011).
53. H. J. Monkhorst and J. D. Pack, Special points for Brillouin-zone integrations, *Physical Review B* 13, 5188 (1976).
54. V. I. Anisimov, J. Zaanen and O. K. Andersen, Band theory and Mott insulators: Hubbard U instead of Stoner I, *Physical Review B* 44, 943 (1991).
55. A. I. Liechtenstein, V. I. Anisimov and J. Zaanen, Density-functional theory and strong interactions: Orbital ordering in Mott-Hubbard insulators, *Physical Review B* 52, R5467 (1995).
56. Y. Zhu, T. Chen, Y. Li, L. Qiao, X. Ma, C. Liu, T. Hu, H. Gao and W. Ren, Multipiezo Effect in Altermagnetic V₂SeTeO Monolayer, *Nano Letters* 24, 472 (2024).
57. A. ullah, D. Bezzerga and J. Hong, Giant spin seebeck effect with highly polarized spin current generation and piezoelectricity in flexible V₂SeTeO altermagnet at room temperature, *Materials Today Physics* 47, 101539 (2024).
58. Zesen Fu, Mengli Hu, Aolin Li, Haiming Duan, Junwei Liu and F. Ouyang, Strain-Controlled Topological Phase Transitions and Chern Number Reversal in Two-Dimensional Altermagnets, *arXiv*:2507.22474 (2025).